Performance Analysis of a Small-Scale Orthopter-Type Vertical Axis Wind Turbine

by

A. ElCheikh[1‡], M. Elkhoury[‡], T. Kiwata[*] , and T. Kono[*]

Orthopter-type Vertical Axis Wind Turbines (O-VAWT) are energy capturing devices which are suitable for micro-generation in urban areas. This paper aims to study the effect of number of blades (solidity), Aspect Ratio (AR), and wind speed on the performance of a small-scale O-VAWT using experimental and numerical techniques. Wind tunnel experiments were carried out to measure the torque of two-, three, and four-bladed turbine, each at a set of different wind speeds and blade aspect ratios. Increasing solidity was achieved by either decreasing the blade aspect ratio or increasing the number of blades, both resulting in a higher peak power coefficient ($C_{p,max}$) of the VAWT. The startup characteristics of the O-VAWT were also examined at different aspect ratios, and showed its capability to start-up even at low wind speeds. In addition, numerical simulations were carried out using an unsteady three-dimensional Delayed Detached Eddy Simulation (DDES) with Spalart Allmaras model. Numerical results of power coefficient were validated by comparison against available experimental data. Moreover, velocity and vorticity contours for the two-, three-, and four-bladed turbines, and pressure contours at different span-wise locations were thoroughly analyzed to link the flow field aerodynamics to relevant changes in power coefficient for different rotor solidities.

Keywords: Orthopter-type Vertical Axis Wind Turbine, Solidity, Delayed Detached Eddy Simulation

‡ School of Engineering, Lebanese American University, P.O.Box: 36 Byblos, Lebanon;
[1] Corresponding author Email: amne.elcheikh@lau.edu.lb
* Institute of Science and Engineering, Kanazawa University, Kanazawa 920-1192, Japan;

1. Introduction

Wind energy has been gaining more popularity as a reliable renewable energy source. Power harvesting has been relying on Horizontal- and Vertical-Axis Wind Turbines. Small-scale designs of the latter have been recently capturing considerable interest due to their capability of harvesting wind energy in all directions at a lower noise levels compared to the HAWTs, making them very suitable candidates for urban areas. In addition, micro-VAWTs are usually placed near obstacles such as buildings and trees, therefore causing unsteadiness in the wind inflow to the turbine. Wekesa et al. [1] conducted a study on the energy content in unsteady winds and concluded that the highest frequency of wind fluctuations suitable for wind turbine applications is 1 Hz. In addition, numerical and experimental studies on the unsteady rotor performance have been investigated by various researchers [2–4].

VAWTs are divided into two main categories, Darrieus-type (D-VAWT), a lift based turbine, and Savonius-type (S-VAWT), which is a drag based turbine. Various configurations of Darrieus- and Savonius-type turbines have been recently investigated by researchers in an attempt to improve their performance. Jin et al. [5] conducted a review on basic experimental and numerical research methods employed to assess the performance of Darrieus Vertical Axis Wind Turbines (D-VAWTs). Bhutta et al. [6] discussed the advantages and disadvantages of different VAWT configurations, including various techniques used to optimize their designs.

Rezaeiha et al. [7] investigated the effect of pitch angle as a potential way to enhance the performance of a VAWT. Computational Fluid Dynamics (CFD) results suggested that this parameter highly influences the load distribution between upwind and downwind halves of the turbine, thereby making dynamic pitching an encouraging approach to optimize the performance. Solidity is yet another important parameter that influences the turbine performance. However, limited studies were dedicated to investigating its effect on the power coefficient and aerodynamic characteristics of the VAWT. There is no clear evidence that the effect of solidity is similar for different VAWT types. In addition, solidity can be manipulated by altering the blade chord length, the blade number or the rotor radius, with no proof that changing any of these parameters will lead to analogous results.

Li et al. [8] performed wind tunnel experiments to understand the effect of solidity at different number of blades on aerodynamic forces around a straight-bladed VAWT. It was concluded that power coefficient decreases when solidity increases, while torque coefficients increase. Similarly, Abu-El-Yazeid et al. [9] investigated the effect of number of blades on the performance of D-VAWT. It was found that the

maximum power coefficient is obtained with the lowest number of blades (2 blades). However, decreasing the number of blades contributes to an increase in the radial cyclic aerodynamic forces, a structurally undesirable effect. Another numerical study aiming to reduce the torque variation by manipulating the number of blades on a D-VAWT was conducted by Raciti Castelli et al. [10]. Similar to the previously-mentioned findings by Abu-El-Yazeid et al. [9] and Li et al. [8] an increase in number of blades causes a decrease in the radial component of the aerodynamic forces. Moreover, an increase in solidity is unfavorable since it results in reducing the power coefficient.

Previous results on the reduction in power coefficient at higher solidities are not in line with the findings of other researchers. Eboibi et al. [11] conducted an experimental investigation of the influence of solidity on the performance of VAWTs. However, unlike previously mentioned studies, solidity was manipulated by altering the blade chord instead of blade number. Authors claimed that irrespective of the parameter altered, the effect of solidity on VAWT performance is similar. It is worth noting that since the chord length directly affects the Reynolds number, hence, the two designs were tested at different velocities to maintain similar Reynolds numbers. Increasing solidity did not affect the peak power output significantly. Nevertheless, the maximum power coefficient is attained at lower Tip Speed Ratio (TSR) for higher solidities. Cheng et al. [12] studied the dynamics of floating straight-bladed VAWT with a number of blades ranging from two to four. The main advantage that was obtained by increasing the number of blades from 2 to 3 is in the reduction of the tower base bending moment, therefore reducing the fatigue damage. Further improvement by increasing the number of blades to 4 was not observed. Furthermore, increasing the chord length results in an increase in the power coefficient up to a maximum value after which it rapidly decreases. Delafin et al. [13] conducted CFD simulations to understand the effect of number of blades and solidity on the performance of Ø-shape VAWT. The number of blades was increased from 2 to 4 while keeping the solidity constant with no observed benefit related to increasing power coefficient. Yet, it is desirable since it results in a decrease in torque, thrust and radial cyclic aerodynamic forces. Subramanian et al. [14] investigated the effect of solidity on the power produced by two and three-bladed small-scale H-type D-VAWTs using three-dimensional CFD simulations. Results showed that the three-bladed configuration having a higher solidity performs better at low tip speed ratios (TSR) due to better interception of blades with wind. On the other hand, vortex-blade interaction at higher TSR reduces the power generation capability of the three-bladed VAWT thereby making lower solidity more favorable.

S-VAWTs are drag-driven devices that perform better than D-VAWTs at low wind speeds. Their solidity is usually altered by changing the number of arc-type blades used. Wenehenubun et al. [15] conducted experiments on one, two, three and four-bladed S-VAWTs. It was concluded that the turbine with highest solidity performs best at lower TSR, but the three-bladed configuration outperforms it at higher TSR. On the contrary, experimental results of Mahmoud et al. [16] showed a better performance for the two-bladed configuration at all TSR. Mao et al. [17] investigated the effect of blade arc angle on the performance of S-VAWT, and concluded that arc angle of 160 degrees produced the highest power coefficient for the studied VAWT configuration.

Unlike D-VAWT and S-VAWTs, Orthepter-type vertical axis wind turbine (O-VAWT) have received very few consideration. In addition, studies focusing on improving their performance are insufficient. Bayeul-Laine et al. [18] confirmed that this type of turbines performs better than classical VAWTs for some specific blade stagger. Two blade shapes (elliptical and straight) were examined with no clear conclusions about a favorable shape could be drawn since the performance is highly dependent on the TSR range. Cooper and Kennedy [19] tested a symmetric-blade O-VAWT design and obtained a maximum power coefficient of 0.25 with a high startup torque, rendering this design favorable for pumping applications. Elkhoury et al. [20] simulated the flow around an Orthopter-type small-scale VAWT (O-VAWT) with three blades. Effects of wind speed and inflow angle on a three-bladed turbine performance were examined.

O-VAWTs possess performance characteristics such as the self-start capability that make them suitable for micro-generation and pumping applications. However, the literature is lacking in studies on O-VAWTs performance. Therefore, the main aim of the present work is to experimentally and numerically investigate the effect of solidity, aspect ratio, and incoming wind speed on the performance of O-VAWTs. The solidity was varied in two different ways: changing the number of blades or changing the chord length. The impact of aspect ratio and wind velocity, previously studied by Elkhoury et al. [20] for a three-bladed O-VAWT, were further extended to include two, and four-bladed turbines. In addition, CFD simulations using DDES were employed to obtain flow patterns of velocity, pressure and vorticity. The analysis of these patterns for different numbers of blades can shed light on changes in flow characteristics due to blade flow interaction.

2. Experimental Description

2.1 Wind tunnel facility

The validity of a numerical study should be assessed by comparison of the results against experimental data. A detailed schematic of the wind tunnel and measurement devices is shown in Fig. 1. The experimental setup used in this work consists of an open-circuit wind tunnel with a square test section of 1.25 m ×1.25 m and a 2.0 m long working section with a bell mouth of 2.00 m. The wind turbine was installed at the center of cross-section 850 mm downstream from the nozzle exit. The turbulence intensity level and flow non-uniformity in the working section at a wind speed of 8 m/s were less than 0.5% and ±1.0%, respectively.

2.2 Rotor models

Fig. 2 shows a photograph and isometric view of the O-VAWT. The O-VAWT tested in the wind tunnel consists of aluminum blades of 1.7 kg each and different thickness of 4, 5 and 6 mm. A chain-and-sprockets arrangement was used to control the pitch angle of the blade. The blades of turbine rotate with a phase difference about their own axis at half the speed of the main rotor. The Reynolds number based on the blade chord at a wind speed of 10 m/s and the blades dimension are summarized in Table 1. It is important to note that a constant blade weight is maintained by changing the thickness so as to maintain a constant load on bearings and to ensure the same inertial effects on start-up characteristics.

Table 1: Blade geometry and Reynolds number at different aspect ratios and incoming wind velocities

	Chord length C	Height h	Thickness t	V = 5 m/s	V = 10 m/s
AR=1.0	0.400 m	0.400 m	4×10^3 m	1.4×10^5	2.8×10^5
AR=1.5	0.290 m	0.434 m	5×10^3 m	1.0×10^5	2.0×10^5
AR=2.0	0.228 m	0.455 m	6×10^3 m	0.8×10^5	1.6×10^5

2.3 Measurement and instrumentation procedures

The main measurement devices consist of an ultrasonic anemometer (Kaijo Sonic, DA-650-3TH & TR-90AH) that is used to measure the speed and temperature of the incoming air flow. The averaged torque T of the turbine was measured by a torque transducer (TEAC TQ-AR5N with a rate capacity of 10 N.m) along with a digital tachometer (ONO SOKKI HT-5500) for measuring the rotational speed, *rpm*,

of the turbine. The output signal of the torque transducer was converted by a 16-bit A/D converter with a sampling intervals of 0.5 degrees, and 36,000 items (50 revolutions) of data were stored. The power coefficient of the turbine was measured at different TSR for constant wind speeds of V = 5 and 10 m/s, by varying the rotational speed of the geared motor (Mitsubishi Electric, GM-S 2.2 kW) accompanied by a variable-frequency inverter (Hitachi, SJ200). The measured values correspond to the total torque including all mechanical losses of bearings and gears. To account for these losses however, the following equation was added to the results of the numerical simulations $C_{p,loss} = 0.0005 - 0.0355\lambda - 0.0502\lambda^2 - 0.3124\lambda^3$ .This equation was obtained using a curve fit of the experimental data with a coefficient of determination R^2 of 0.9999. The uncertainty levels of measurements were estimated to around 2% for the ultrasonic anemometer, ± 0.03 N**.** m for the torque transducer, and around 1% for the tachometer, respectively. The uncertainty of maximum power coefficient at V = 10 m/s was approximately estimated to be ± 0.05C_p.

3. Numerical Model

3.1 Turbulence Model

CFD simulations were performed by employing the DDES based on the Spalart Allmaras (SA) turbulence model. DDES falls in the category of hybrid Reynolds-Averaged-Navier-Stokes/Large-Eddy-Simulation (RANS/LES) models, which is capable of achieving higher accuracy than RANS models for complex flows with less computational cost when compared to LES. The choice of the DDES based on the SA model stems from the fact that it was successful in modeling aeronautical applications involving massive flow separation [21], not to mention the lower computational cost associated with solving a single transport equation. In addition, the model has a linear near-wall behavior of its transport property, requiring mesh densities as low as those used with algebraic models [22].

3.2 Computational Domain

3.2.1 Geometry and Mesh

To account for complex flow structures associated with various aspect ratios, a 3-D approach is considered in the present study, which allows to model the central shaft along with the connecting rods. It is worth noting that all modeled turbines are simpler than those of the experiment, where gears and chains are omitted for the purpose of improving the mesh quality and solver's convergence time with minimal

effect on the results. The different turbines shown in Fig. 2 have similar structure, where each blade is attached to the rotor by two connecting rods, and the latter are connected to the blade by the means of two blade holders. Thus, each blade is allowed to rotate around its center with an angular velocity of $-\omega/2$ relative to its rotation around the rotor as indicated in Fig. 2. As depicted in Tables 2 and 3, ten turbines are analyzed, each of the two- and three-bladed VAWTs are simulated with three different aspect ratios of 1, 1.5 and 2 while the four-bladed one is only simulated with the aspect ratios 1.5 and 2 since interference/intervention among blades occurs at AR=1. For the first eight turbines shown in Table 2, the aspect ratio was altered by changing both the blade chord and height while maintaining constant blade swept area as defined in Fig. 2. Moreover, two additional turbines with constant height and varying blade chord as shown in Table 3 were tested. The diameter of all considered rotors is 51 cm. The 3-D investigation of such turbines requires a segmentation of the domain into the far field, turbine and blades domains as depicted in Fig. 3. Each blade domain comprises of a rotating cylinder that is encapsulated by the turbine's domain being a rotating domain as well. The full assembly is engulfed by the far field that represents the fluid flowing around the VAWT.

Table 2: Solidities and swept areas for turbines with different aspect ratios and number of blades

	N=2	N=3	N=4
AR=1.0 (C=0.4m, H=0.4m)	$\sigma = 0.50$ A=0.284	$\sigma = 0.749$ A=0.284	----
AR=1.5 (C=0.29m, H=0.435m)	$\sigma = 0.362$ A=0.284	$\sigma = 0.543$ A=0.284	$\sigma = 0.724$ A=0.284
AR=2.0 (C=0.228m, H=0.456m)	$\sigma = 0.285$ A=0.284	$\sigma = 0.427$ A=0.284	$\sigma = 0.570$ A=0.284

Table 3: Solidities and swept areas for turbines with different blade chord lengths

	N=3
AR=0.89 (C=0.449m, H=0.4m)	$\sigma = 0.841$ A=0.294
AR=1 (C=0.4m, H=0.4m)	$\sigma = 0.749$ A=0.284
AR=1.06(C=0.377m, H=0.4m)	$\sigma = 0.706$ A=0.279

3.2.2 Far Field

As stated earlier, this domain is equivalent to the wind tunnel where the fluid flows across from one end to another. It is worth noting that the dimensions are carefully selected in order to prevent any interference that may lead to inaccurate results based on the recommendations of Rezaeiha et al. [23]. Therefore, the turbine is placed at a distance of 11.37 D from the inlet and 12.13 D from the outlet, and midway from the other boundaries in the transverse and rotor axial direction as depicted in Fig. 3. A Boolean operation takes place to subtract the rotating domains from the fixed one to create separate entities. Thus, an interface boundary condition is assigned at the intersection of the two domains so the turbine can rotate around its center while allowing a smooth flow between the two. An unstructured coarse mesh is applied since the geometry is of simple shape and flow characteristics in this region are not supposed to change. Moreover, identical sizing functions are enforced at the interfaces to ensure a smooth transmission between the two without incurring any loss due to interpolation of data.

3.2.3 Rotor Domain

In addition to being a rotating domain, this field encompasses the full geometry, such as the blades, connecting rods, and rotor. For simplicity purposes, the turbine excluding the blades is removed from this area leaving thin surfaces with no slip boundary condition, in return this reduces the number of elements and accelerates the solver's convergence. Similarly, the blade domains are deducted from the rotating volume while an interface is set at the intersection to ensure continuity of the flow between the different domains and allow each domain to rotate together and relative to each other. Hence, when an angular velocity ω around the z-axis is allocated to the domain, both the turbine and blade domains follow the same path at the same rate. Additionally, a fine unstructured mesh is applied given the complexity of the geometry. Identical sizing function is also imposed at the interfaces of the rotating cylinders to obtain a good transition between the domains without jeopardizing the accuracy of the results.

3.2.4 Blade Domain

As mentioned earlier, each blade is enclosed by a cylinder that is separated from the turbine domain since this VAWT is characterized by their variable pitch mechanism. The blades are deducted from their

enclosures and removed, consequentially a thin surface with non-slip boundary condition remains covering the boundaries of all blades. This in return, reduces the mesh density and helps in accelerating the solver's convergence. This set-up allows for the blade to rotate around its mid center with an angular velocity of -ω/2, and around the turbine's center with an angular velocity of ω, as stated previously. Seeing that the blades are the most important parts of a VAWT, The finest unstructured mesh is applied to the blades at this level along with inflation layers adjacent to their surfaces as they comprise the most important part of a VAWT. Hence, complex flow structures near the blade's wall can be accurately resolved, which in turn increases the reliability of the results.

4 Validation

4.1 Mesh Dependency Study

Mesh dependency study is crucial for insuring accurate results. Therefore, simulations on the four-bladed turbine with $AR = 2$, $V = 5$m/s and $TSR = 0.40$ were carried out using different mesh resolutions. After convergence was obtained for an initial mesh, referred to herein as "Regular mesh", the grid was further refined in the turbine and blade domains and iterations were performed until solution converged to the set criterion of 1×10^{-4} of scaled residual. Specifications of both grids are delineated in Table 4. The criterion used to confirm that the solution is mesh independent is the change in the averaged power coefficient C_p. As depicted in Fig. 4, the variation in C_p between regular and fine mesh solutions is less than 2% in averaged power coefficient. Therefore, any further refinement of the mesh is not justified in terms of accuracy, and has a disadvantage of increasing the computational cost. It is worth to note that 10 to 15 layers of inflation prisms were placed around all solid surfaces with the first off-surface node located within a range of $1\times$ to 5×10^{-6} m, resulting in values of $y+ \leq 1.0$.

Table 4: Regular and fine grid specifications for mesh dependency study

Domain	Regular Mesh	Fine Mesh
Blade 1 CV	1,610,660	3,785,943
Blade 2 CV	1,614,903	3,808,216
Blade 3 CV	1,588,363	3,768,389
Blade 4 CV	1,614,661	3,799,238
Turbine CV	2,127,497	3,879,281
Far Field	441,196	441,196
Total Cell Number	8,997,280	19,482,263

4.2 Time Step Study

For the same geometry and regular grid density of the preceding section, the initial time step used was $\Delta t = 5\times10^{-5}$s corresponding to the time needed for the turbine to accomplish a rotation angle of 0.045 degrees at TSR = 0.4, and resulting in a CFL ≤1.0 adjacent to the rotor and in wake regions. This condition was maintained throughout the computations to ensure proper scale-resolving simulations. This time step was further reduced to half of this initial value. Fig. 5 depicts the variation of power coefficient for both time steps. The maximum percentage difference in C_p is less than 0.56%. Hence, the larger time step was adopted since it minimizes the computational cost while retaining good accuracy levels. The averaging process of C_p values started after the elapse of the initial two revolutions and continued over the following six to eight revolutions, which were enough to obtain statistical convergence [24].

4.3 Flow Solver and Boundary Conditions

A commercial CFD solver, Ansys® Fluent® 17.2, was utilized to solve the equations of motion. An unsteady coupled pressure-based double precision solver was employed. A second order bounded central difference discretization scheme was adopted for the momentum equations whereas a second order upwind-based discretization scheme was selected for flow variables of the SA model. Numerical instabilities resulting from the use of central difference scheme were avoided by adopting the bounded central difference scheme. The latter is more robust compared to the former due to its slight numerical dissipation however, is sufficiently low to allow turbulent structures to evolve. Flow gradients were discretized using the Least Square Cell Based approach. A second order central difference pressure interpolation scheme, which reconstructs the pressure values at cell faces, was selected. A second order implicit scheme was employed for transient formulation. Default under-relaxation factors of 1.0 for density, body force, and turbulent viscosity, and 0.8 for the modified turbulent viscosity were employed. The default explicit-relaxation factor of 0.75 was adopted for momentum and pressure. The solver was utilized in a parallel mode with 14 processors, 112 cores of Intel®-Xeon®-CPU-E5-2667-v3-@-3.2GHz. A typical revolution on these cores consumed around 23 hrs of computational time on the regular mesh.

All considered test cases fall within the incompressible flow regime and thus, the following boundary conditions were employed. A velocity inlet boundary condition was implemented at the inlet where a uniform inflow velocity was assumed. The inlet pressure was extrapolated upstream from the computation

zone. At the outlet, the pressure outlet boundary condition was implemented where an outlet static gauge pressure of zero was specified. All other flow variables were extrapolated from interior cells. A symmetry boundary condition was implemented in the transverse and axial directions as indicated by Fig. 3. Gradients of all flow variables are set to zero on these boundaries, thereby neglecting blockage effect. Based on the work of Rezaeiha et al. [25], it was found that a blockage ratio of less than 5% had negligible effect on the predicted power performance of the turbine. It is worth to note that a blockage ratio of 1.29% based on the swept area of the rotor, A, and the domain cross sectional area (5D ×17D) was obtained for the current configuration, justifying the use of a symmetry boundary condition. The no-slip and condition was applied at all solid boundaries.

5 Results

5.1 Effect of Chord and Number of Blades (Solidity) on Performance

Solidity is one of the main parameters that affect the power produced by the turbine. Manipulating solidity is usually achieved by varying the number of blades or the blade chord length. Different experimental approaches could be used to measure the power coefficient, the torque transducer was employed in this work. Fig. 6 compares the averaged power coefficient variation with TSR for VAWTs with different number of blades, but similar aspect ratios, at two different wind speeds. The trend in C_p-TSR curves is similar to the experimental results of the D- and S-VAWTs as presented by Li et al. [8], Eboibi et al. [11], and the numerical results of Consul et al. [26]. The power coefficient increases with TSR, until it attains a peak value, after which it begins to decrease. In the region past the peak TSR value, the rate at which C_p decreases is affected by solidity. Higher solidities result in faster decrease in C_p values. Fig. 6 results also show a shift in the C_p-TSR curves towards lower TSR values when the number of blades increases. This is further confirmed in Fig. 7 where the TSR at which maximum C_p occurs is plotted for all tested VAWT models. Adding more blades to the VAWT results in reaching the maximum C_p at lower TSR. In addition, the operating range of the VAWT increases at lower solidities. This finding is in agreement with the results of Eboibi et al. [11] and Consul et al. [26] which showed that one of the consequences of lowering solidity of a D-VAWT is a wider range of the C_p-TSR curve. The effect of solidity on the maximum output power of the turbine could be inferred from Fig. 8. It is clear that the peak power coefficient produced increases with the number of blades. Increasing the number of blades from 2 to 3 results in a 10% increase in peak power coefficient at V = 5m/s, and 35% at V = 10 m/s. Moreover,

the four-bladed architecture produces a higher C_p compared to the three-bladed one at both tested wind velocities. On the contrary, increasing the VAWT solidity by solely increasing the blade chord length does not lead to similar results. As shown in Fig. 9, the VAWT with highest solidity produces more power at all TSR. However, the change in solidity did not cause any shift in the peak of C_p-TSR curve towards lower TSR as observed when manipulating the number of blades. However, it is worth noting that the range of maximum increase in solidity when changing c from 378 to 445 mm is 17%, which is much lower than the 50% increase obtained when changing the number of blades from 2 to 3.

In order to assess the ability of the DDES model to predict the performance of the VAWT, CFD simulation were performed at a velocity of 10 m/s for all turbines, the results of which are shown in Fig. 6 (d, e and f). The maximum deviation from experimental data occurs at or slightly off the peak power coefficient. Discrepancies between experimental and numerical results could be associated with the simplifications in the modeled geometry and/or accuracy of selected model, a point that merits further investigation.

5.2 Effect of Aspect Ratio and Wind Speed on Performance

In the previous section, results regarding the performance of O-VAWTs with different blade chord length were discussed to infer the effect of solidity. Additionally, changing chord length also leads to a change in aspect ratio. Nevertheless, the range of aspect ratios that could be achieved without changing the blade height is short, and consequently the obtained difference in C_p was within the uncertainty of the measurements weakening the judgement regarding the effect of aspect ratio on the power produced by the turbine. Therefore, additional experiments were carried out for different combinations of c and h, so that a wider range of aspect ratios is studied and shown in Fig. 6. Combinations of c and h were chosen such that the turbine swept area (A) is conserved for all tested VAWT models. By examining the results shown in Fig. 7a and b, it can be concluded that the impact of aspect ratio on the speed at which $C_{p,max}$ occurs does not show clear trends. For the two- and four-bladed designs, increasing the aspect ratio did not affect the location of the maximum C_p at both wind velocities. Furthermore, increasing the aspect ratio while keeping the same number of blades lowers the peak power coefficient as shown in Fig. 8. Such behavior was observed by Zanforlin et al. [27] for small straight-bladed VAWT at low Reynolds number and was attributed to the increase in Reynolds number implied by the chord extension. Therefore, at higher wind speeds (V=10 m/s), the favorable effect of increasing the Reynolds number is counteracted by the

detrimental growth in losses due to tip vortices, and the growth in C_p at lower AR is less important. Nevertheless, this behavior is in contradiction with the findings of Abulyazied et al. [9] and Raciti Castelli et al. [10] for D-VAWTs. Consequently, increasing solidity by either increasing number of blades or decreasing aspect ratio (chord) is favorable for increasing the power produced by the VAWT.

It can also be inferred by comparing Fig. 6 (a and d, b and e, c and f) that the power coefficient increases with wind speed. Additionally, the range in which positive values of C_p are maintained is much wider at higher wind velocities. It is also worth noting that the difference in power coefficients at wind speed of 5 m/s between the two- and three-bladed designs is not significant. However, the four-bladed design shows an average increase of 40% in $C_{p,max}$. On the contrary, the increase in C_p at a wind speed of 10 m/s by increasing the number of blades from 2 to 3 is substantial (around 35% increase in $C_{p,max}$), while it is less significant for a further increase in number of blades from 3 to 4. The TSR corresponding to a maximum C_p increases with wind speed, which is in agreement with the results of Elkhoury et al. [20] for a three-bladed O-VAWT.

5.3 Effect of Solidity on Turbine Start-Up Characteristics

Wind turbines could be used as standalone power generation systems or in hybrid mode with other renewable or non-renewable energy sources. When employed to supply electricity in remote areas, the ability of the wind turbine to self-start at low wind speeds is crucial. D-VAWTs have low starting torque and therefore are not suitable for such applications. On the other hand, S-VAWTs have good self-starting characteristics, but fail to achieve high power coefficients. In Fig. 10, the power coefficient of the O-VAWT is compared to that of a S-VAWT tested by Blackwell [28], both having an aspect ratio of 1 at an incoming wind velocity of 7 m/s. The O-VAWT is able to achieve a higher peak C_p than the S-VAWT and at lower TSR. In addition, Elkhoury et al. [20] showed that the O-VAWT has the ability to self-start at wind speeds as low as 1.3 m/s and thus, outperforming the S-VAWT which self-starts at 2 to 6 m/s wind speeds.

Solidity has a strong impact on the self-starting characteristics of the VAWT. As pointed out in the previous section, solidity could be varied by changing either the number of blades or the blade chord length. Elkhoury et al. [20] thoroughly investigated the effect aspect ratio manipulated by changing both the blade chord and height. It was concluded that the O-VAWT with AR=1 not only starts at lowest wind

speeds, but also attains high TSR at lower wind speeds when compared to the turbines with AR equal 1.5 and 2. In Fig. 11, the effect of changing the blade chord while retaining same height on the turbine self-start wind speed is shown. Similar superior self-starting behavior of the VAWT with lowest aspect ratio (highest chord and solidity) is observed. Fig. 12 shows the effect of number of blades on the turbine startup characteristics. The three-bladed configuration is able to start at a wind speed less than 2 m/s, thereby outperforming the two- and four-bladed VAWTs. However, the turbine with lowest solidity (N=2) has a sharper increase in TSR making it able to achieve higher tip speed ratios than three- and four-bladed turbines for wind speeds greater than 2 m/s.

Hybrid D/S-VAWT configurations are the subject of many recent studies [29–31]. The main aim of this configuration is to take benefit of the high C_p of D-VAWT and the good self-starting characteristics of the S-VAWT. Fig. 13 shows the power coefficient variation with TSR of a three-bladed O-VAWTs with AR=1 and a three-bladed D-VAWT previously studied by Elkhoury et al. [32]. A hybrid O/D-VAWT configuration could have promising performance characteristics in terms of startup torque and peak C_p. However, further investigations are required to assess the viability of such configurations.

Moreover, it is worth noting that the current study results were generated assuming uniform incoming air flow, while in real conditions, the incoming flow is turbulent and unsteady. Wekesa et al. [2] investigated the aerodynamic performance of a small-scale S-VAWT operating in an external turbulent inflow. When a turbulent inflow was introduced, an improvement in the startup characteristics of the turbine was observed and was attributed to the reduction of the relative velocity between the rotor and the incoming wind. However, further investigation on the performance of the O-VAWT under unsteady wind conditions is required to confirm its superior self-starting characteristics in real life applications.

5.4 Blade Flow Interaction

In order to explain the observed differences in performance of O-VAWTs with different number of blades, flow patterns of velocity and vorticity were closely examined at an aspect ratio of 1.5 and a wind velocity of 10 m/s. The patterns were obtained from numerical simulations which were previously validated by comparing average C_p values at different tip speed ratios to experimental results. Fig. 14 shows the instantaneous out-of-plane vorticity contours on a mid-plane cutting through the turbine blades for 30 degrees blade rotation increments. The flow around blades oriented at 0, 30, and 60 degrees does

not interact with the flow features produced by neighboring blades. Therefore, for the two-, three- and four-bladed turbine, the instantaneous contours of vorticity are similar. At 90 degrees, a Leading Edge Vortex (LEV) develops for all turbines. However, it is smallest for the turbine with highest solidity. Moreover, the flow patterns around the 180 degree oriented blades in Fig. 14 (a, b and c) indicate higher concentration of positive and negative vorticity patches in the absence of neighboring blades. When neighboring blades are present as in the case of the three-bladed and four-bladed turbines, the flow becomes more constrained and therefore small vorticity patches tend to combine into a bigger patch on the trailing edge of the blade. Therefore, the energy extraction capability of the turbine is enhanced by adding more blades. When linking this result to the performance of the turbine, the higher power coefficient for the higher solidity turbines can be explained. The formation of rollup vortex with negative vorticity is observed at 270 degrees for the two-bladed turbine in Fig. 14j and at 210 degrees for the three and four-bladed turbines shown in Fig. 14 (k and l). The rollup vortex continues to grow until the azimuthal angle becomes 300 degrees. At this point, the layer of vortices from the neighboring blades interacts with the rollup vortex and results in breaking it up into several smaller vorticity patches. Differences in flow patterns between the two and three-bladed VAWTs are very prominent, while the three and four-bladed turbines have similar flow features. It is worth noting that the discrepancy in C_p between the two turbines of higher solidities is low, while the lowest solidity turbine produces much lower power coefficients than both. Therefore, observations on instantaneous flow patterns are in perfect agreement with average power coefficient results.

Mid-plane contours of velocity magnitude for the same configuration are depicted in Fig. 15. An examination of these contours around blades oriented at different azimuthal angles reveals interesting aspects of the flow. The flow around 0 and 30 degree oriented blades for the range of solidities considered is indistinguishable. At 60 degrees (Fig. 15b, g and i), the appearance of a region of high velocity at the blade leading edge indicates the formation of the leading edge vortex described earlier. The fastest growth of the LEV is observed on the lower solidity turbine due to the absence of close neighboring blades. At 210 degrees (Fig. 15f), the wake region from the trailing edge of the blade interacts with the LEV and causes its detachment from the blade surface. In addition, the wake regions on blades oriented at 180 degrees and higher cover the entire blade surface for the three- and four-bladed O-VAWTs. Therefore, the drag force is higher for turbines of higher solidities. In general, O-VAWTs can be designed to be lift or drag-driven depending on the blade cross-sectional shape. The configuration tested in the present study has a flat cross-section and is therefore drag-driven. In addition, the presence of big regions of low velocity

for the higher solidity turbines confirms the attainment of higher C_p as they extract the flow energy better than the two-bladed configuration.

5.5 Three-Dimensional Flow Characteristics

In order to better understand the effects of blade aspect ratio and number of blades on the performance of the turbine, three-dimensional flow characteristics were closely examined at an incoming wind speed of 10 m/s and a TSR of 0.4. Since the flow features on each blade change as it rotates, a careful selection of the azimuthal angle of the blade, on which flow characteristics will be examined, is required. Fig. 16 (a, b and c) shows Iso-surfaces of pressure at 70 Pa colored by velocity magnitude in the flow direction and pressure contours at different span-wise locations on the blade for the two-bladed turbine with AR of 1. A LEV develops on the blade oriented at 60 degrees as shown in Fig. 16a. As the blade rotates to achieve an azimuthal angle of 120 degrees, the LEV is entrained downstream and tip vortices appear on the upper and lower edges of the blade. However, the effect of tip vortices is restricted towards the blade edges ($\mu = 0.98$). It is also worth noting that the LEV remains attached to the blade surface at all span-wise locations. At 180 degrees, the tip vortices are elongated, and about to be shed into the freestream. Moreover, their effect stretches from blade edge to the midspan location causing a separation of the LEV from the blade surface at $\mu = 0$. Since it is interesting to investigate flow features along the blade when vortices are prominent and separation phenomenon occurs, theazimuth angle of 180 degrees was selected to examine the impact of AR and blade number on flow features.

Fig. 17 (a, b and c) also shows Iso-surfaces of pressure at 70 Pa colored by velocity magnitude in the flow direction and pressure contours at different span-wise locations on the blade for the two-bladed turbine having AR equal 1, AR equal 2, and the three-bladed turbine having AR equal 1 respectively. For all three VAWTs, tip vortices are generated due to the pressure difference between the pressure side and suction side of the blade causing the flow to curl along the blade tip towards the suction side. However, by comparing Fig. 17 (a and b), it is evident that tip vortices are more prominent on shorter blades having low AR. Additionally, vortices on the high AR blade seem to be fed by the large gap between the blade edge and the turbine shaft, while vortices on the low AR blade strongest near the leading edge of the blade. The impact of higher Reynolds number associated with shorter blades counteracts the high tip losses and therefore lower aspect ratios are favorable for the small-scale O-VAWT tested in this work. In addition,

pressure contours confirm that tip losses are lowest at midspan ($\mu = 0$) where highest C_p is attained [33], therefore highlighting the negative effect of the three-dimensional nature of the flow on the VAWT performance. Another comparison between Fig. 17 (a and c) could be made to investigate the impact of number of blades on the turbine performance. The addition of a third blade to the turbine results in more concentrated vortices, without causing substantial changes in the flow structures. Nevertheless, the additional blade is favorable for extracting more power from the incoming wind. However, careful investigations are required to confirm the effect of adding extra blades. Similar conclusions could be drawn by examining Fig. 18 (a, b and c). The streamlines along blades having same azimuthal angle reveal a stronger rollup of vortices associated lower AR blade, and no noticeable impact of adding a third blade on the flow characteristics.

6 Conclusions

O-VAWTs with number of blades ranging from 2 to 4, and aspect ratios of 0.899, 1, 1.06, 1.5 and 2, were tested in a wind tunnel at wind speeds of 5 and 10 m/s. Additionally, DDES using Spalart Allmaras model were performed at the latter wind speed. Following a close agreement between CFD and experimental results, the effect of solidity, aspect ratio and wind speed on the turbine performance was examined. The major findings are summarized below:

1- The maximum power coefficient attained by the turbine increases with solidity. However, the range of TSR for which the turbine maintains positive C_p is wider for turbines of lower solidities. In addition, the tip speed ratio at which $C_{p,max}$ occurs decreases for O-VAWTs with higher number of blades (solidity), but does not show consistent behavior for increased solidity by means of chord length.
2- An increase in aspect ratio, while retaining the same number of blades, results in a decrease in $C_{p,max}$. Nevertheless, no clear trend on the variation of the tip speed ratio at which $C_{p,max}$ occurs with aspect ratio could be inferred from the results.
3- The TSR corresponding to $C_{p,max}$ increases at higher wind speeds.
4- The O-VAWT is able to start-up at lower wind speeds compared to a typical S-VAWT. Moreover, decreasing solidity by increasing aspect ratio is favorable for improving the start-up at low wind speeds.

5- For an incoming wind speed of 10 m/s, differences in instantaneous flow structures between the two- and three- bladed turbines were substantial and therefore, leading to a significant change in the average power coefficient produced. On the other hand, the flow around three- and four- bladed turbines showed similar features, resulting in smaller change in the average C_p at all tip speed ratios.

6- Three-dimensional flow characteristics reveal that the effect of tip losses on reducing the power coefficient of the turbine having lower AR is counteracted by the increase in Reynolds number due to chord extension.

The present work on O-VAWTs sheds light on the effect of different parameters on its performance under uniform inflows. Although turbulent inflows usually enhances the output power of the turbine, it is recommended to conduct further studies to confirm its ability to withstand the increase in aerodynamic loads under such conditions. In addition, hybrid configurations of O/D-VAWTs are believed to possess the self-starting ability of O-VAWT and the energy capturing capabilities of the D-VAWT at high wind speeds. Therefore, future work will be extended to developing and testing such wind turbine configurations.

References

[1] D.W. Wekesa, C. Wang, Y. Wei, L.A.M. Danao, Analytical and numerical investigation of unsteady wind for enhanced energy capture in a fluctuating free-stream, Energy. 121 (2017) 854–864. doi:10.1016/j.energy.2017.01.041.

[2] D.W. Wekesa, C. Wang, Y. Wei, W. Zhu, Experimental and numerical study of turbulence effect on aerodynamic performance of a small-scale vertical axis wind turbine, J. Wind Eng. Ind. Aerodyn. 157 (2016) 1–14. doi:10.1016/j.jweia.2016.07.018.

[3] L.A. Danao, J. Edwards, O. Eboibi, R. Howell, A numerical investigation into the influence of unsteady wind on the performance and aerodynamics of a vertical axis wind turbine, Appl. Energy. 116 (2014) 111–124. doi:10.1016/j.apenergy.2013.11.045.

[4] D.W. Wekesa, C. Wang, Y. Wei, J.N. Kamau, L.A.M. Danao, A numerical analysis of unsteady inflow wind for site specific vertical axis wind turbine: A case study for Marsabit and Garissa in Kenya, Renew. Energy. 76 (2015) 648–661. doi:10.1016/j.renene.2014.11.074.

[5] X. Jin, G. Zhao, K. Gao, W. Ju, Darrieus vertical axis wind turbine: Basic research methods, Renew. Sustain. Energy Rev. 42 (2015) 212–225. doi:10.1016/j.rser.2014.10.021.

[6] M.M. Aslam Bhutta, N. Hayat, A.U. Farooq, Z. Ali, S.R. Jamil, Z. Hussain, Vertical axis wind turbine - A review of various configurations and design techniques, Renew. Sustain. Energy Rev. 16 (2012) 1926–1939. doi:10.1016/j.rser.2011.12.004.

[7] A. Rezaeiha, I. Kalkman, B. Blocken, Effect of pitch angle on power performance and aerodynamics of a vertical axis wind turbine, Appl. Energy. 197 (2017) 132–150. doi:10.1016/j.apenergy.2017.03.128.

[8] Q. Li, T. Maeda, Y. Kamada, J. Murata, K. Shimizu, T. Ogasawara, A. Nakai, T. Kasuya, Effect of solidity on aerodynamic forces around straight-bladed vertical axis wind turbine by wind tunnel experiments (depending on number of blades), Renew. Energy. 96 (2016) 928–939. doi:10.1016/j.renene.2016.05.054.

[9] T.G. Abu-el-yazied, A.M. Ali, M.S. Al-ajmi, I.M. Hassan, Effect of Number of Blades and Blade Chord Length on the Performance of Darrieus Wind Turbine, Am. J. Mech. Eng. Autom. 2 (2015) 16–25.

[10] M. Castelli, S. De Betta, E. Bernini, Effect of Blade Number on a Straight-Bladed Vertical Axis Wind Turbine, World Acad. Sci. Eng. Technol. 61 (2012) 305–311.

[11] O. Eboibi, L.A.M. Danao, R.J. Howell, Experimental investigation of the influence of solidity on the performance and flow field aerodynamics of vertical axis wind turbines at low Reynolds numbers, Renew. Energy. 92 (2016) 474–483. doi:10.1016/j.renene.2016.02.028.

[12] Z. Cheng, H.A. Madsen, Z. Gao, T. Moan, Effect of the number of blades on the dynamics of floating straight-bladed vertical axis wind turbines, Renew. Energy. 101 (2017) 1285–1298. doi:10.1016/j.renene.2016.09.074.

[13] P. Delafin, T. Nishino, L. Wang, A. Kolios, Effect of the number of blades and solidity on the performance of a vertical axis wind turbine, J. Phys. Conf. Ser. 753 (2016) 022033. doi:10.1088/1742-6596/753/2/022033.

[14] A. Subramanian, S.A. Yogesh, H. Sivanandan, A. Giri, M. Vasudevan, V. Mugundhan, R.K. Velamati, Effect of airfoil and solidity on performance of small scale vertical axis wind turbine using three dimensional CFD model, Energy. 133 (2017) 179–190. doi:10.1016/j.energy.2017.05.118.

[15] F. Wenehenubun, A. Saputra, H. Sutanto, An experimental study on the performance of Savonius wind turbines related with the number of blades, Energy Procedia. 68 (2015) 297–304. doi:10.1016/j.egypro.2015.03.259.

[16] N.H. Mahmoud, A.A. El-Haroun, E. Wahba, M.H. Nasef, An experimental study on improvement of Savonius rotor performance, Alexandria Eng. J. 51 (2012) 19–25. doi:10.1016/j.aej.2012.07.003.
[17] J.H. Lee, Y.T. Lee, H.C. Lim, Effect of twist angle on the performance of Savonius wind turbine, Renew. Energy. 89 (2016) 231–244. doi:10.1016/j.renene.2015.12.012.
[18] B.-L. Annie-Claude, S. Sophie, D. Aurore, B. Gérard, Numerical study of flow stream in a mini VAWT with relative rotating blades, 2010 (2010) 1–13.
[19] P. Cooper, O.C. Kennedy, P. Cooper, O. Kennedy, Development and Analysis of a Novel Vertical Axis Wind Turbine Development and Analysis of a Novel Vertical Axis Wind Turbine, Proc. Sol. 2004 Life, Universe Renewables. (2004) 1–9.
[20] M. Elkhoury, T. Kiwata, K. Nagao, T. Kono, F. ElHajj Wind tunnel experiments and Delayed Detached Eddy Simulation of a three-bladed micro vertical axis wind turbine, Renew. Energy. doi.org/10.1016/j.renene.2018.05.096.
[21] M. Shur, P.R. Spalart, M. Strelets, A. Travin, Detached-eddy simulation of an airfoil at high angle of attack, in: Eng. Turbul. Model. Exp. 4, Elsevier, 1999: pp. 669–678. doi:10.1016/B978-008043328-8/50064-3.
[22] P. SPALART, S. ALLMARAS, A one-equation turbulence model for aerodynamic flows, in: 30th Aerosp. Sci. Meet. Exhib., American Institute of Aeronautics and Astronautics, Reston, Virigina, 1992. doi:10.2514/6.1992-439.
[23] A. Rezaeiha, H. Montazeri, B. Blocken, Towards accurate CFD simulations of vertical axis wind turbines at different tip speed ratios and solidities: Guidelines for azimuthal increment, domain size and convergence, Energy Convers. Manag. 156 (2018) 301–316. doi:10.1016/j.enconman.2017.11.026.
[24] P. Ouro, T. Stoesser, An immersed boundary-based large-eddy simulation approach to predict the performance of vertical axis tidal turbines, Comput. Fluids. 152 (2017) 74–87. doi:10.1016/j.compfluid.2017.04.003.
[25] A. Rezaeiha, I. Kalkman, B. Blocken, CFD simulation of a vertical axis wind turbine operating at a moderate tip speed ratio: Guidelines for minimum domain size and azimuthal increment, Renew. Energy. 107 (2017) 373–385. doi:10.1016/j.renene.2017.02.006.
[26] C. a Consul, R.H.J. Willden, E. Ferrer, M.D. McCulloch, Influence of Solidity on the Performance of a Cross-Flow Turbine, Proc. 8th Eur. Wave Tidal Energy Conf. Uppsala, Sweden. (2009) 484–493.
[27] S. Zanforlin, S. Deluca, Effects of the Reynolds number and the tip losses on the optimal aspect ratio of straight-bladed Vertical Axis Wind Turbines, Energy. 148 (2018) 179–195. doi:10.1016/j.energy.2018.01.132.
[28] R.E. Sheldahl, L.V. Feltz, B.F. Blackwell, Wind tunnel performance data for two- and three-bucket Savonius rotors, J. Energy. 2 (1978) 160–164. doi:10.2514/3.47966.
[29] R. Gupta, R. Das, K.K. Sharma, Experimental Study of a Savonius- Darrieus Wind Machine, Int. Conf. Renew. Energy Dev. Ctries. (2006) 1–11. http://www.udc.edu/docs/cere/Gupta.pdf.
[30] X. Liang, S. Fu, B. Ou, C. Wu, C.Y.H. Chao, K. Pi, A computational study of the effects of the radius ratio and attachment angle on the performance of a Darrieus-Savonius combined wind turbine, Renew. Energy. 113 (2017) 329–334. doi:10.1016/j.renene.2017.04.071.
[31] T. Wakui, Y. Tanzawa, T. Hashizume, T. Nagao, Hybrid configuration of darrieus and savonius rotors for stand-alone wind turbine-generator systems, Electr. Eng. Japan (English Transl. Denki Gakkai Ronbunshi). 150 (2005) 13–22. doi:10.1002/eej.20071.
[32] M. Elkhoury, T. Kiwata, E. Aoun, Experimental and numerical investigation of a three-

dimensional vertical-axis wind turbine with variable-pitch, J. Wind Eng. Ind. Aerodyn. 139 (2015) 111–123. doi:10.1016/j.jweia.2015.01.004.

[33] B. Yang, C. Lawn, Three-dimensional effects on the performance of a vertical axis tidal turbine, Ocean Eng. 58 (2013) 1–10. doi:10.1016/j.oceaneng.2012.09.020.

List of Tables

List of Figures

631 **Nomenclature**

AR : Aspect ratio of blade (= h/c)
A : *Turbine swept area (= [D + c/2] h)*
C_p : Turbine power coefficient (= $T\omega /0.5\rho V^3$A)
$C_{p,max}$: Maximum pressure coefficient
C : Blade chord length
D : Turbine diameter
h : Blade span length
I : Turbulence intensity (= u'/V)
l : Turbulent length scale
N : Number of blades
R : Turbine radius
Re : Reynolds number
T : Turbine torque
TSR : Tip speed ratio ($\lambda = R\omega / V$)
V : Wind speed
y^+ : Dimensionless wall distance
ρ : Air density
σ : Turbine solidity (=$Nc/2\pi R$)
ω : Turbine angular velocity (= $2\pi rpm/60$)
μ : Non-dimensional span-wise position

632

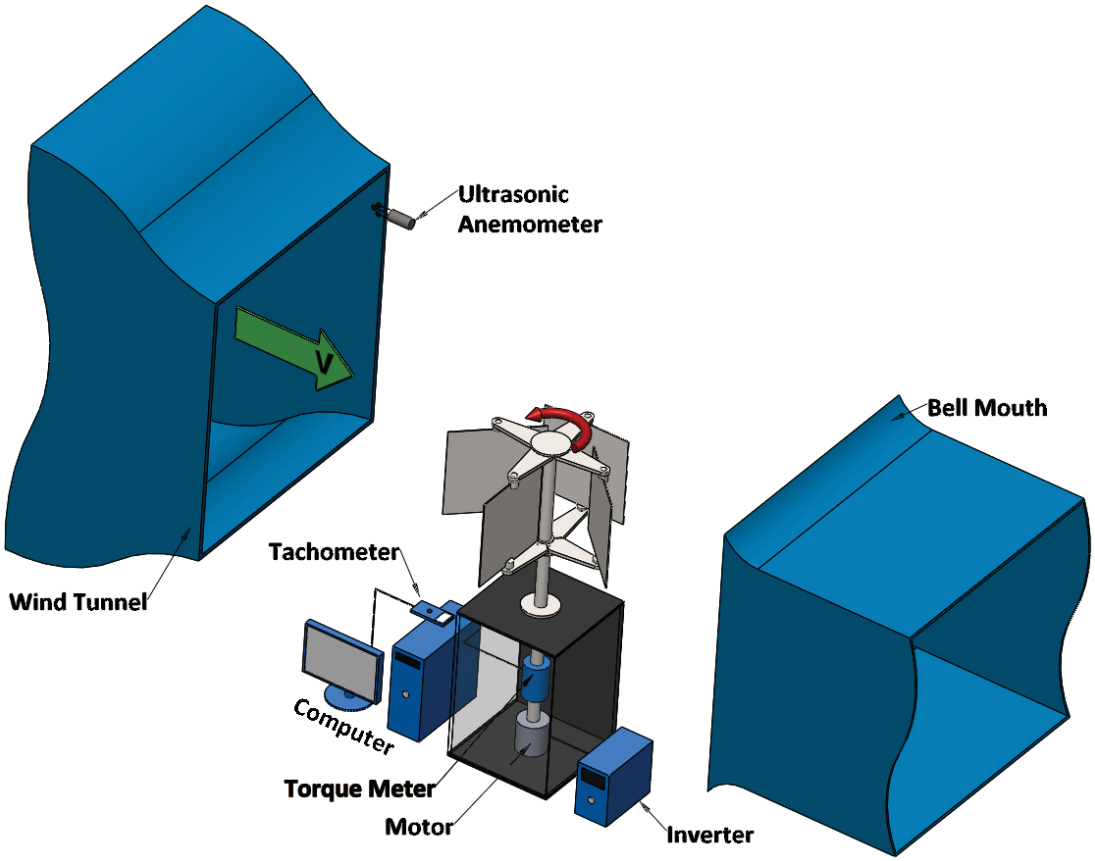

633

634

635 **Figure 1: Schematic diagram of the wind tunnel and the experimental apparatus.**

636

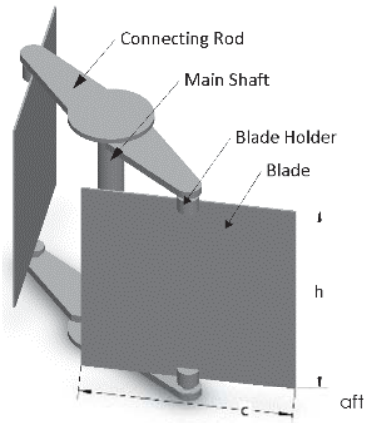
Connecting Rod
Main Shaft
Blade Holder
Blade
h
t
c
aft

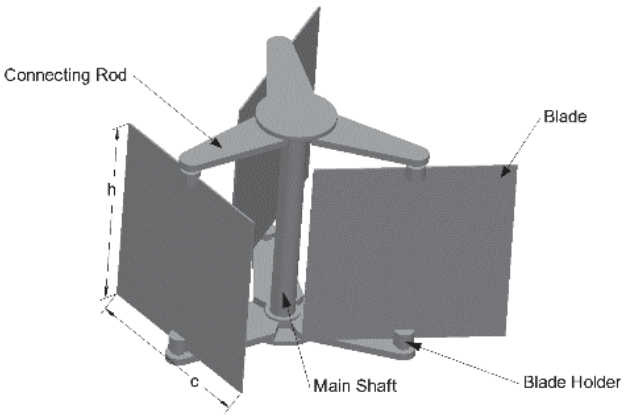
Connecting Rod
Blade
h
c
Main Shaft
Blade Holder

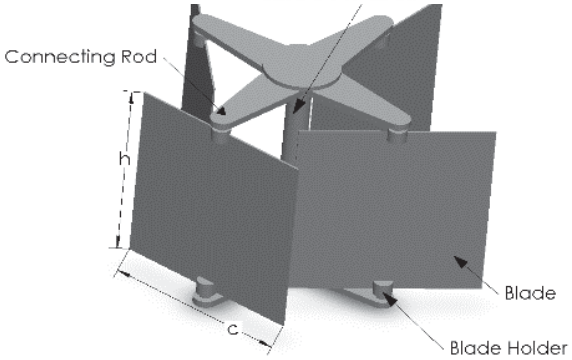
Connecting Rod
h
Blade
c
Blade Holder

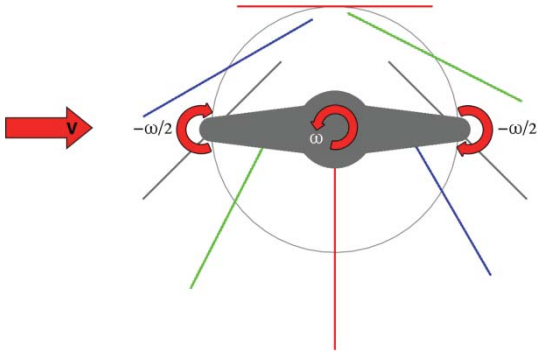
V
−ω/2
ω
−ω/2

637

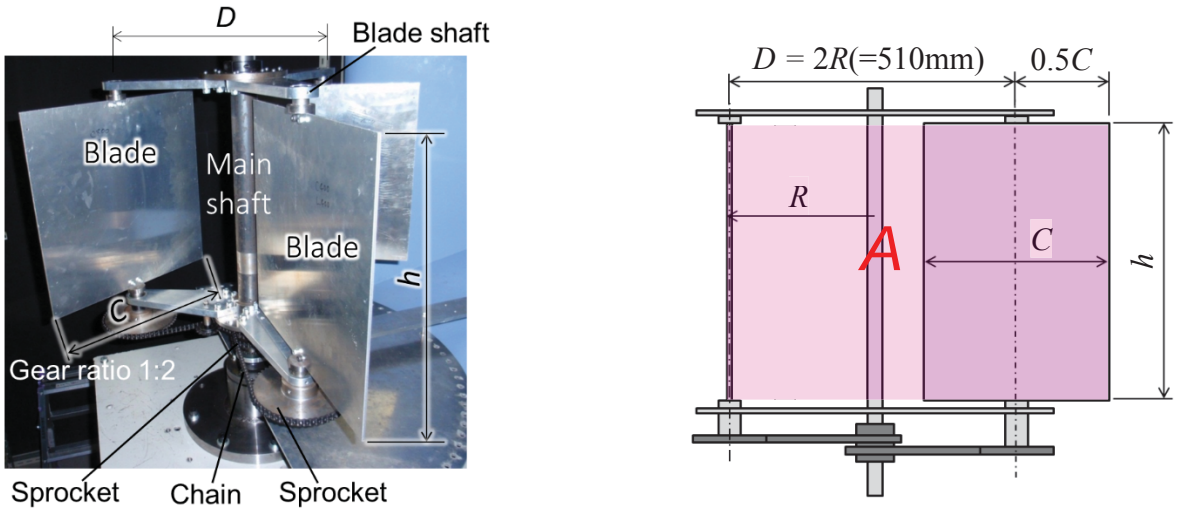

Figure 2: Isometric view of the three rotors and top view of the two-bladed rotor showing blade motion.

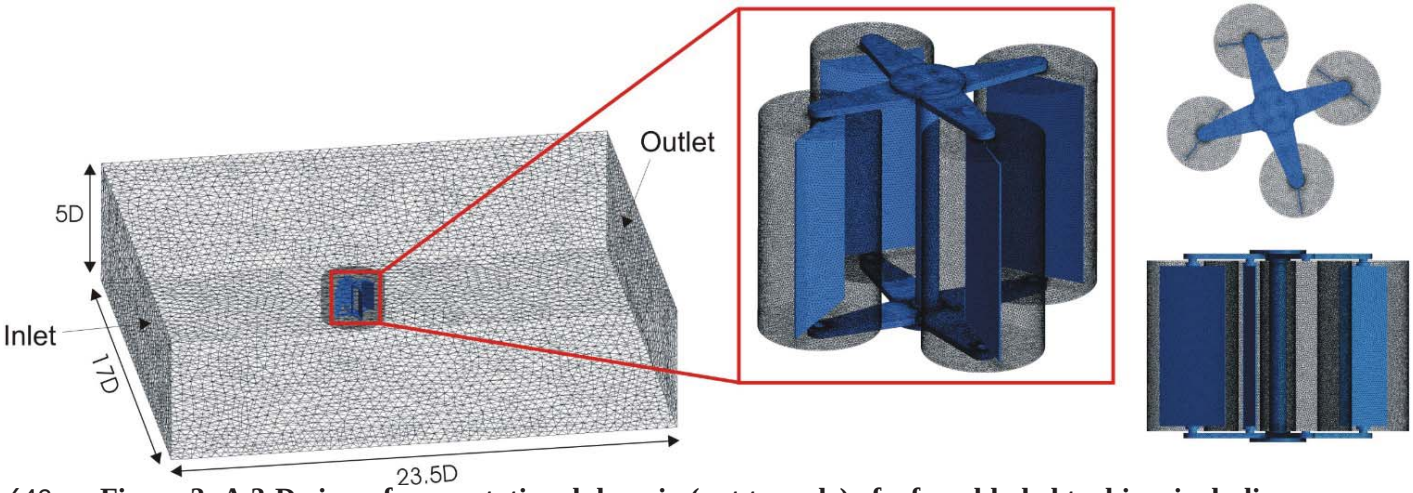

Figure 3: A 3-D view of computational domain (not to scale) of a four-bladed turbine, including an isometric, top, and side view of rotor.

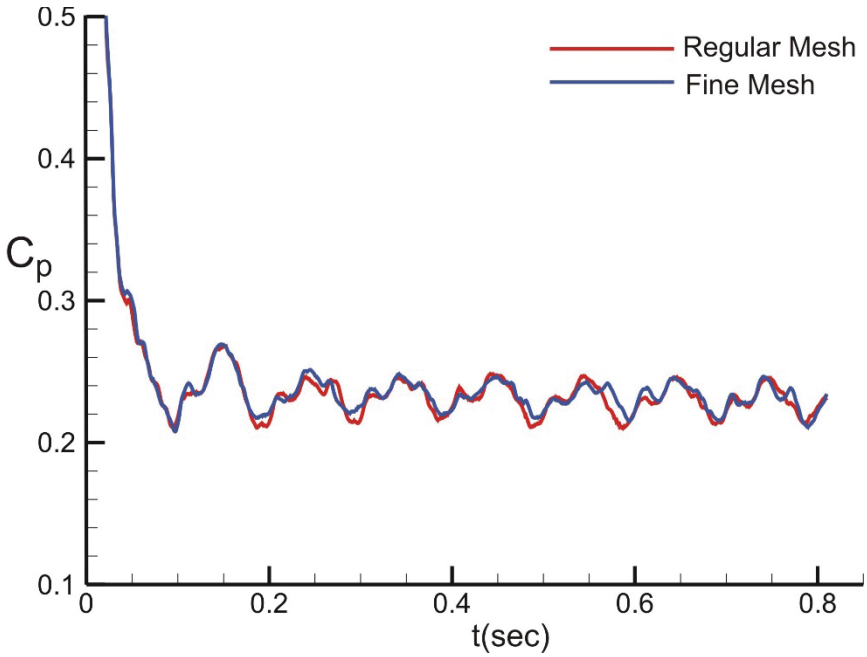

Figure 4: Effect of mesh density on the accuracy of the predicted power coefficient.

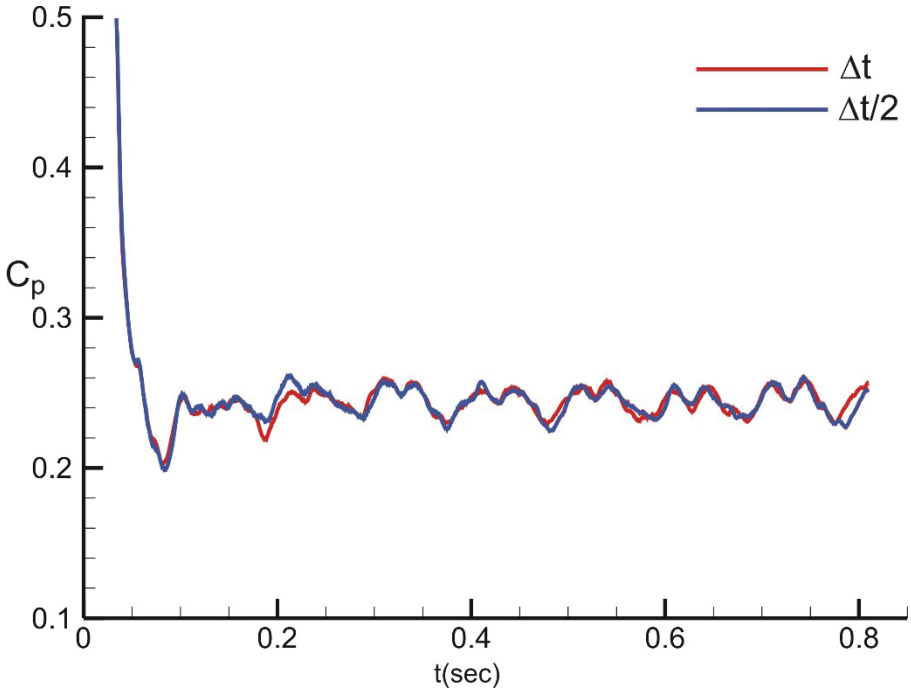

Figure 5: Effect of time-step on the accuracy of the predicted power coefficient.

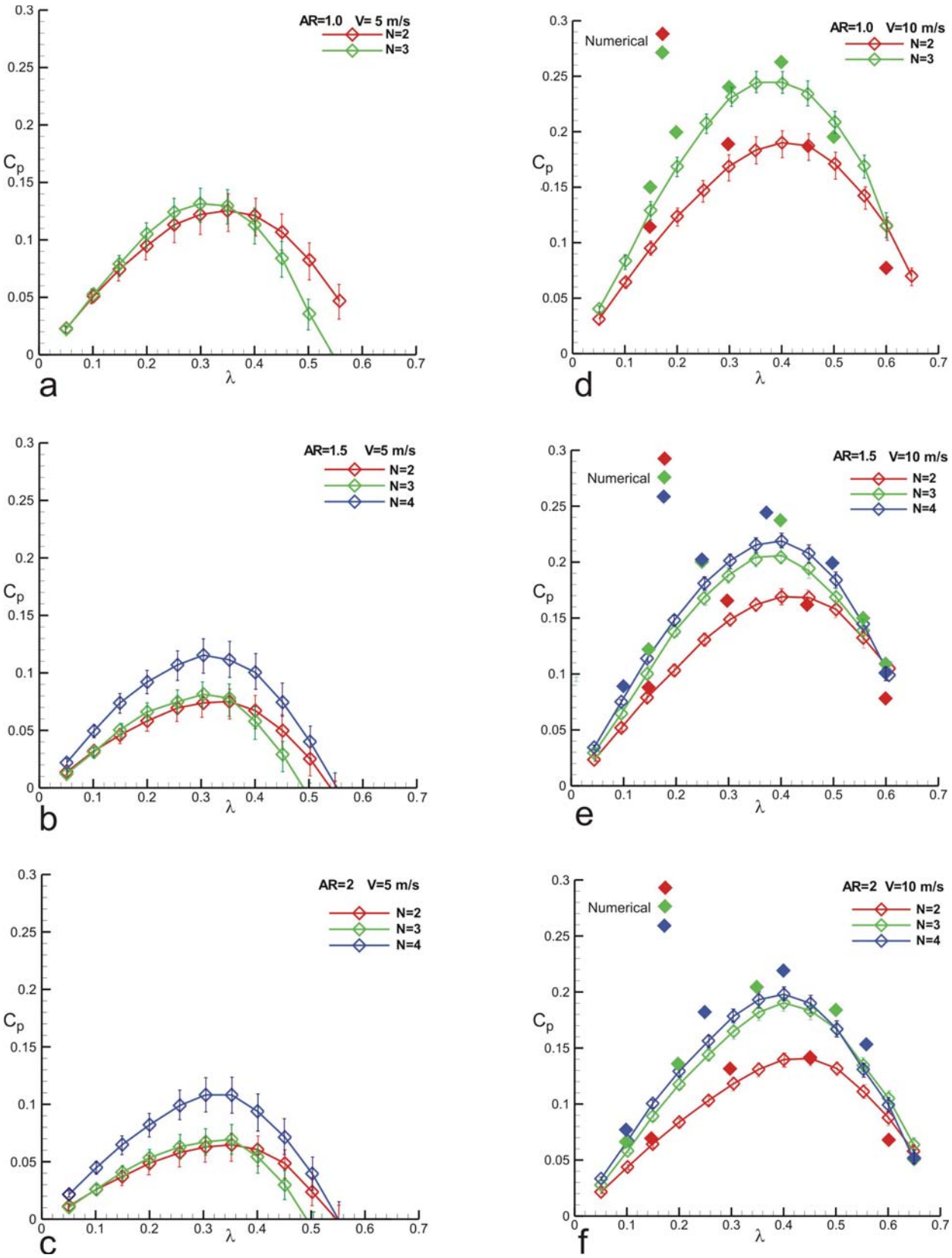

Figure 6: Effect of Aspect Ratio, number of blades (Solidity), and wind speed on the average power coefficient of O-VAWT.

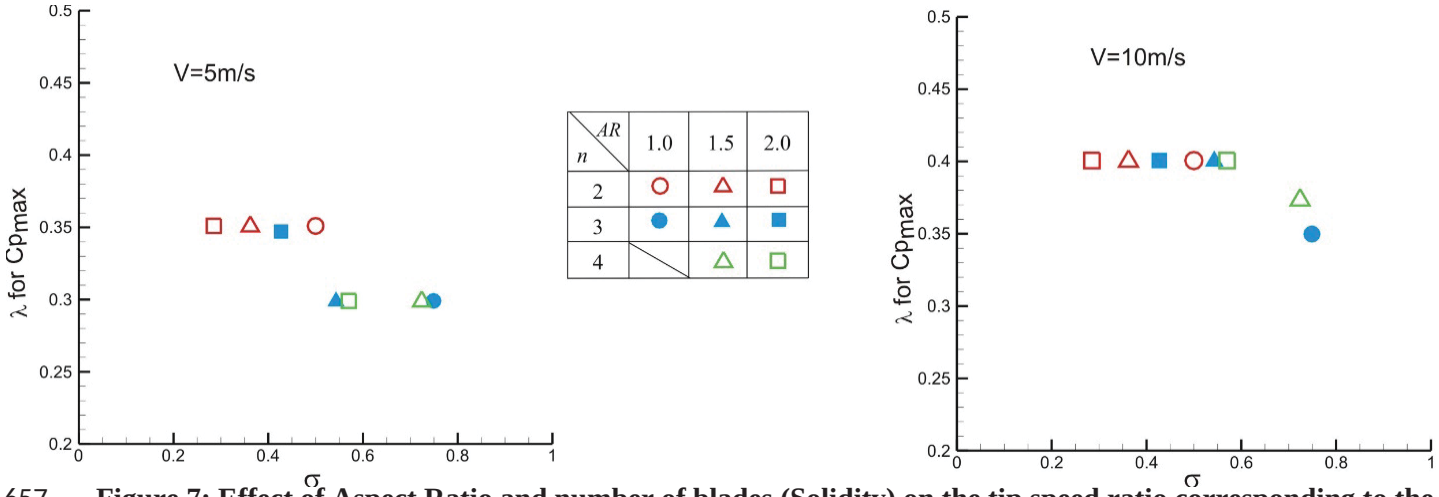

Figure 7: Effect of Aspect Ratio and number of blades (Solidity) on the tip speed ratio corresponding to the maximum power coefficient of O-VAWT at a) V=5m/s, and b) V=10m/s.

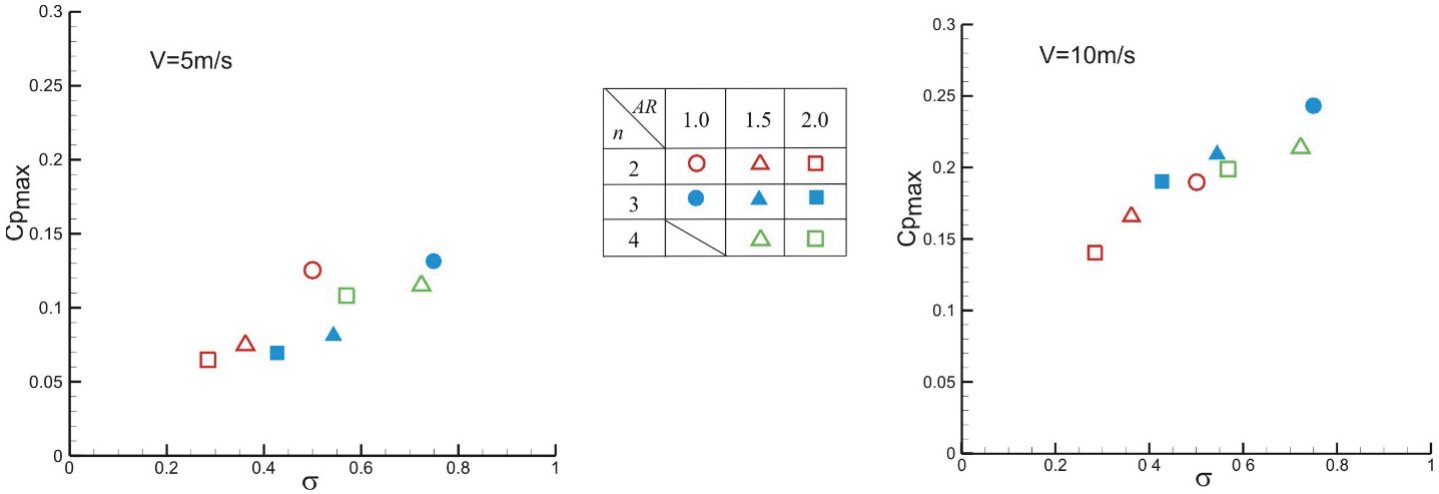

Figure 8: Effect of Aspect Ratio and number of blades (Solidity) on the maximum power coefficient of O-VAWT at a) V=5m/s, and b) V=10m/s.

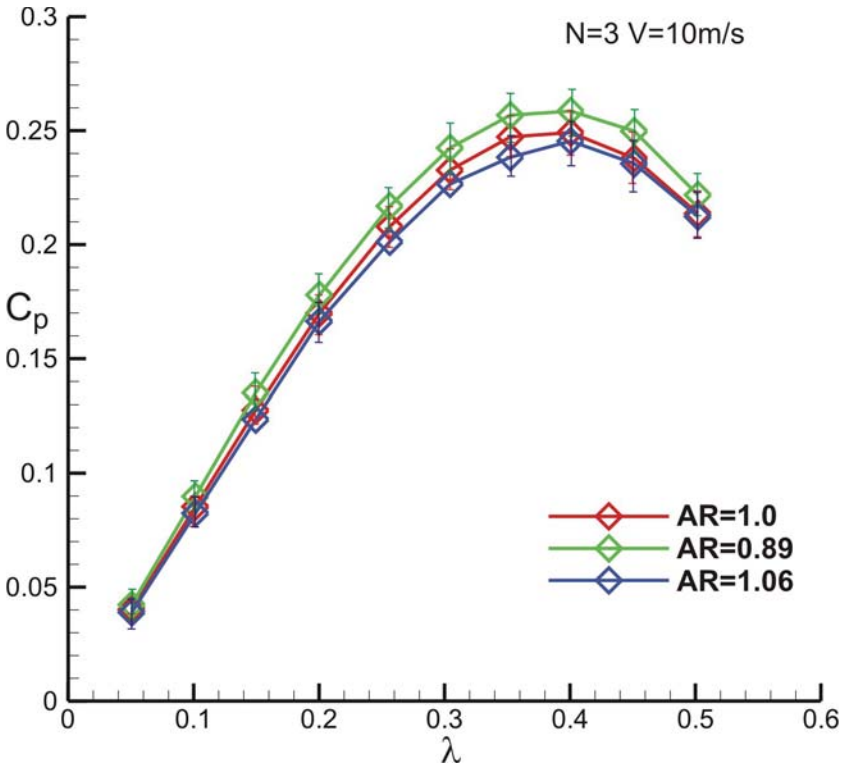

Figure 9: Effect of chord length on the averaged power coefficient of the O-VAWT

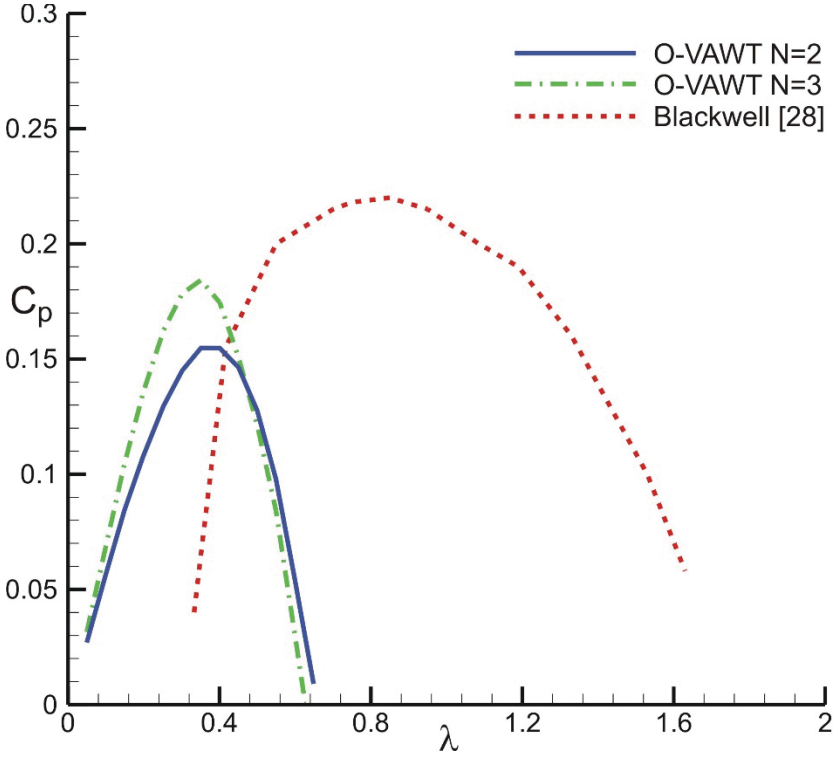

Figure 10: A comparison of C_p vs. TSR between O-type and S-type VAWTs.

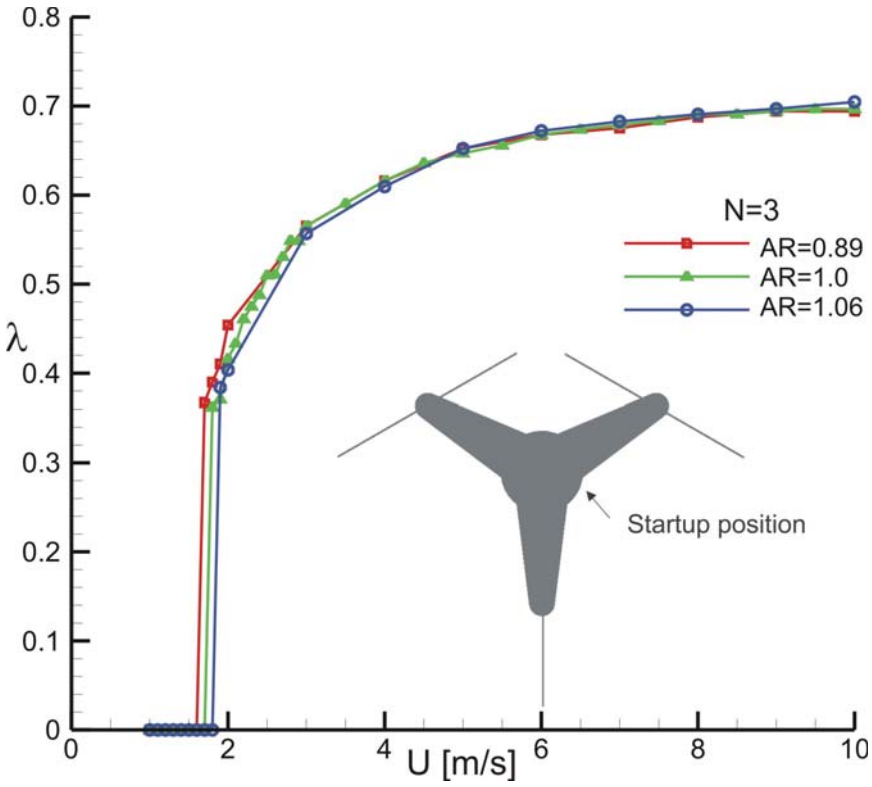

Figure 11: Effect of chord length on the start-up of the O-VAWT.

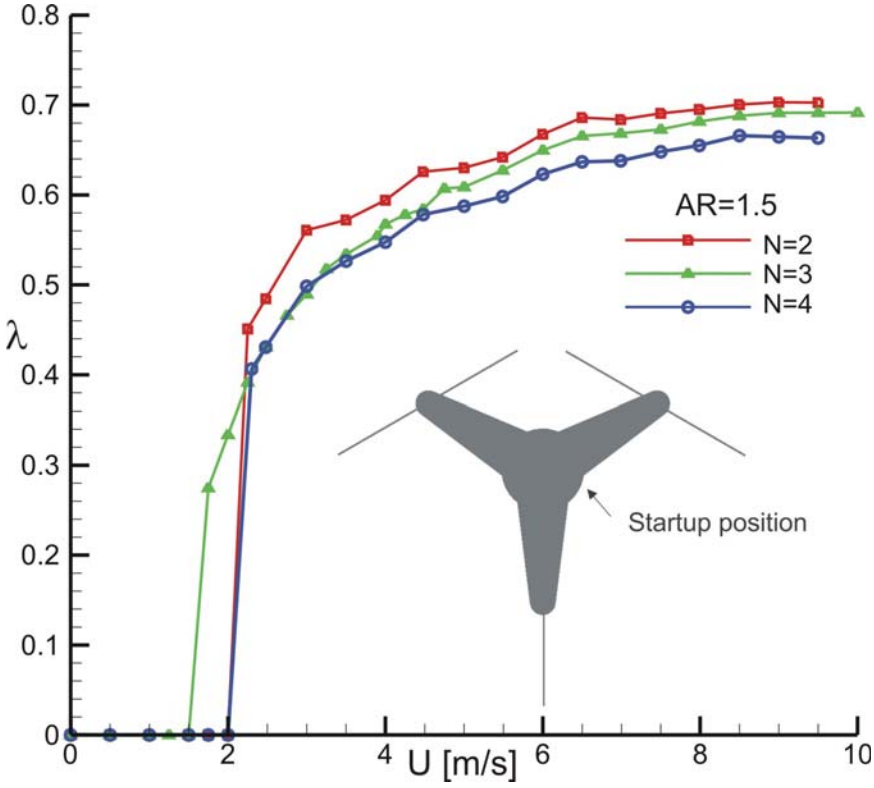

Figure 12: Effect of number of blades on the start-up of the O-VAWT.

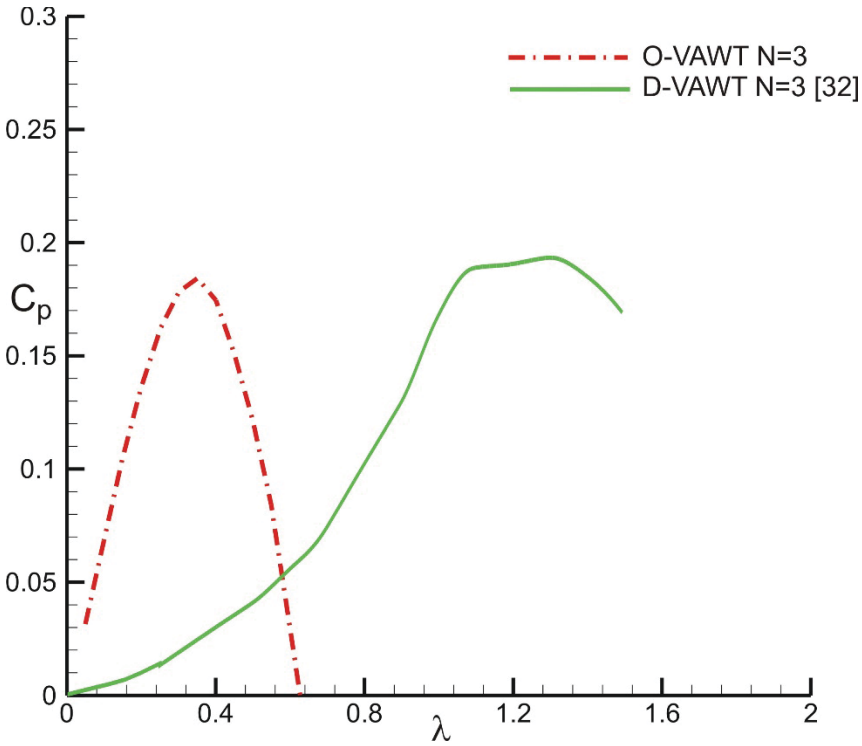

672

673 **Figure 13: A comparison of C_p vs. TSR between O-type and D-type VAWTs.**

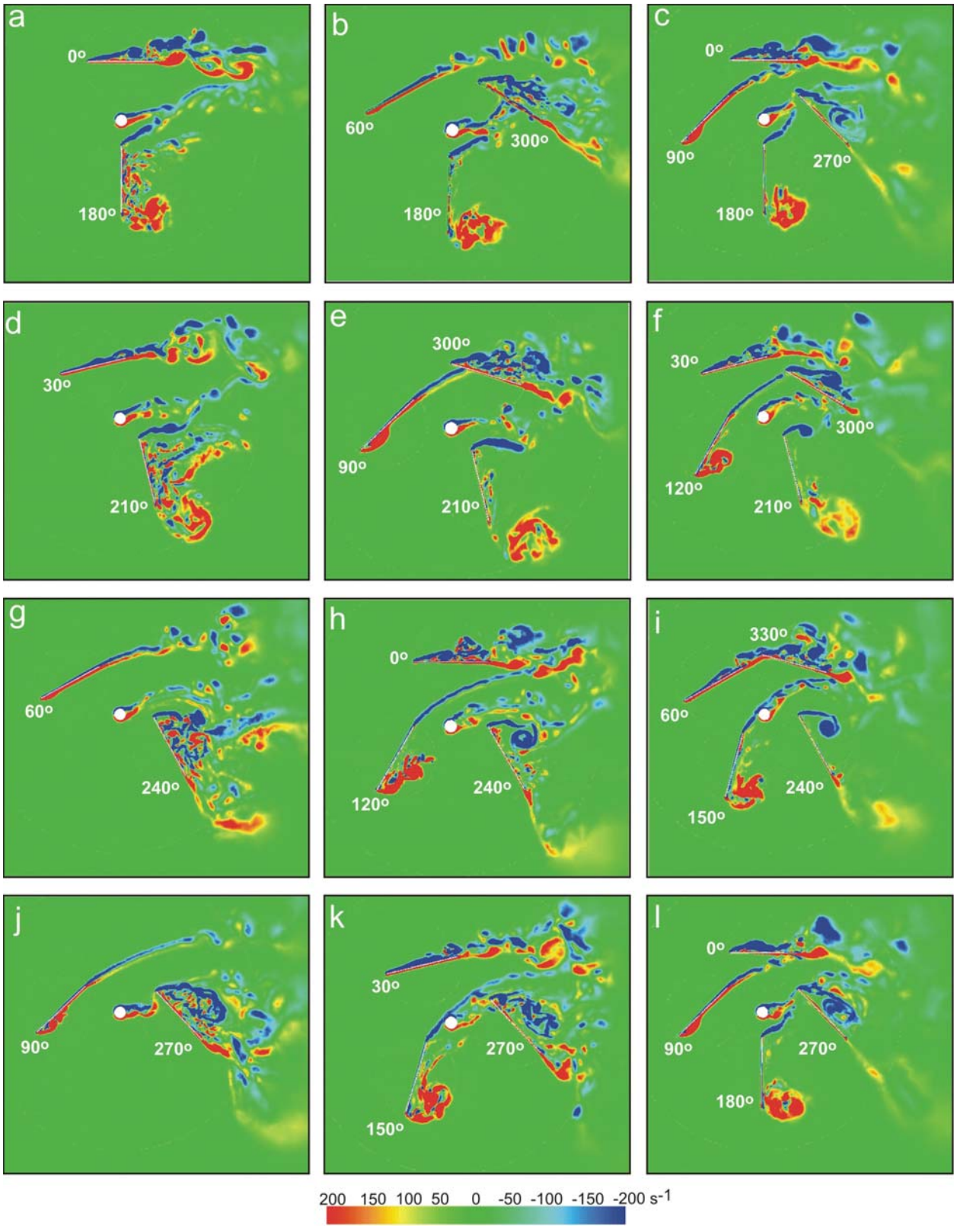

674

675 **Figure 14: Instantaneous out-of-plane vorticity field on a mid-plane of O-VAWT at TSR=0.4 and wind**
676 **speed of 10 m/s for three different rotors**

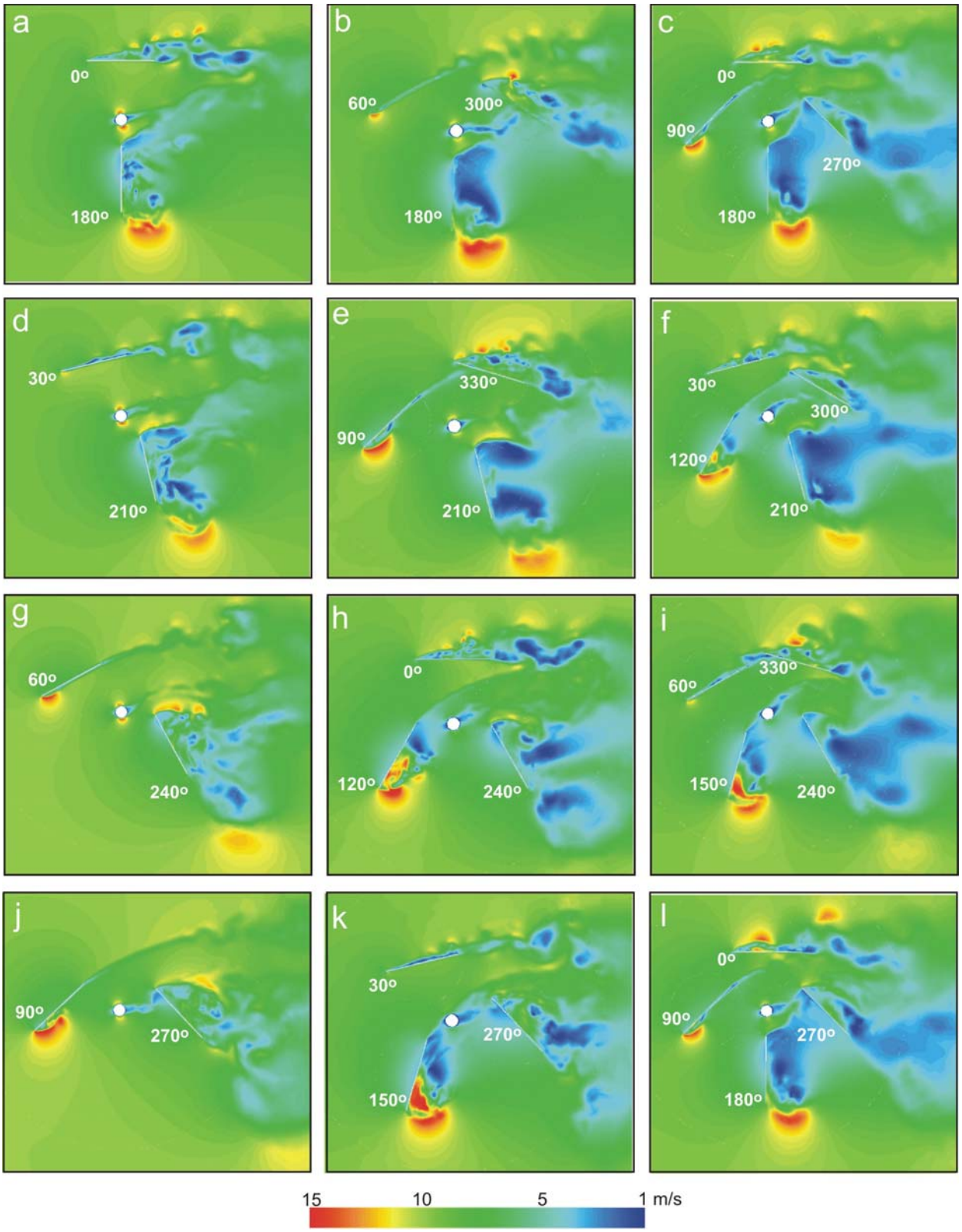

677

678 **Figure 15: Instantaneous velocity magnitude field on a mid-plane of O-VAWT at TSR=0.4 and wind speed**
679 **of 10 m/s for three different rotors.**

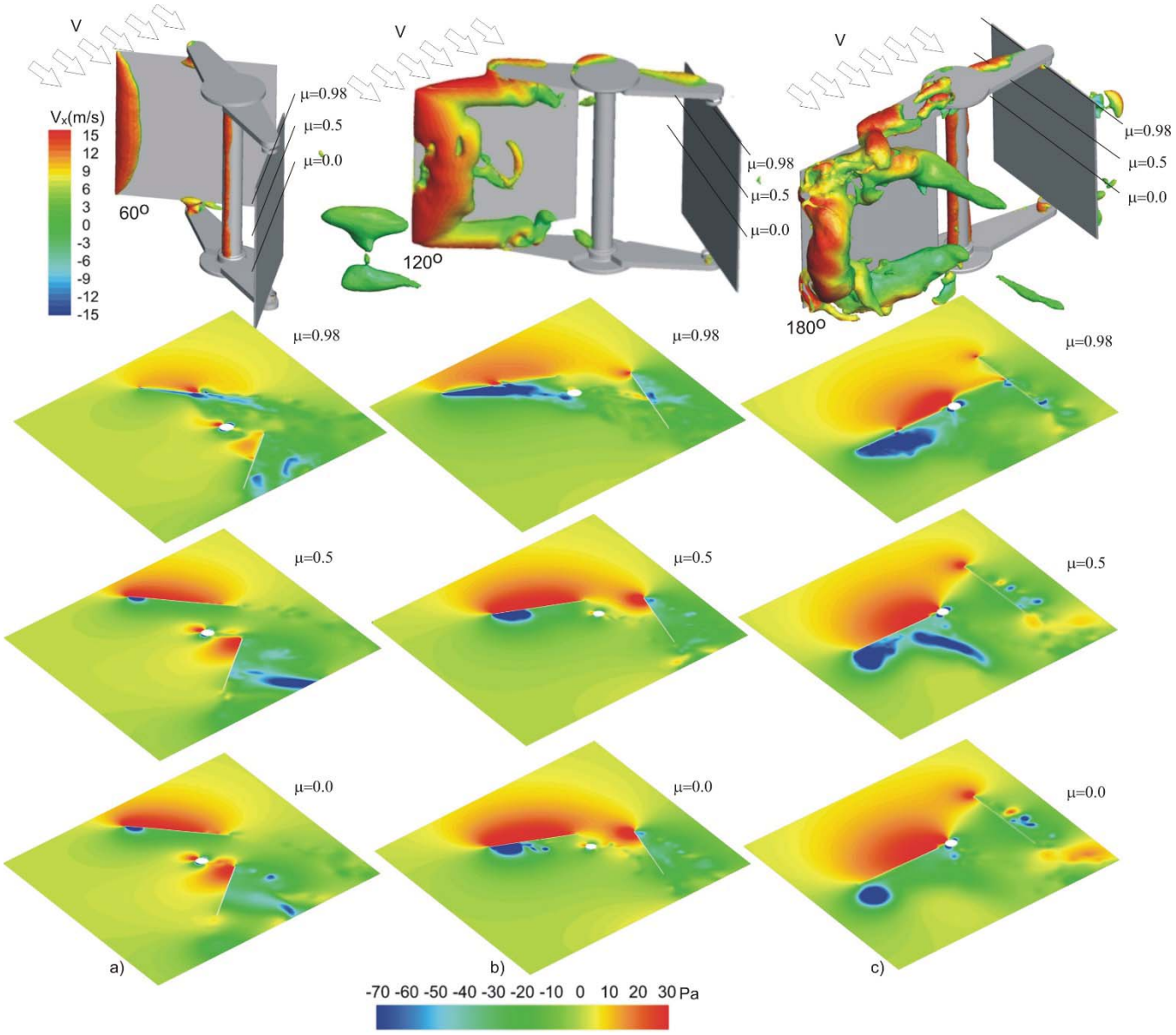

680

681 **Figure 16:** Instantaneous pressure Iso-surface of 70 Pa and pressure field on planes at different span-wise
682 locations of the two-bladed O-VAWT (AR=1) at TSR=0.4 and wind speed of 10 m/s for different blade azimuthal
683 positions. a) 60^{o} b) 120^{o} c) 180^{o}.

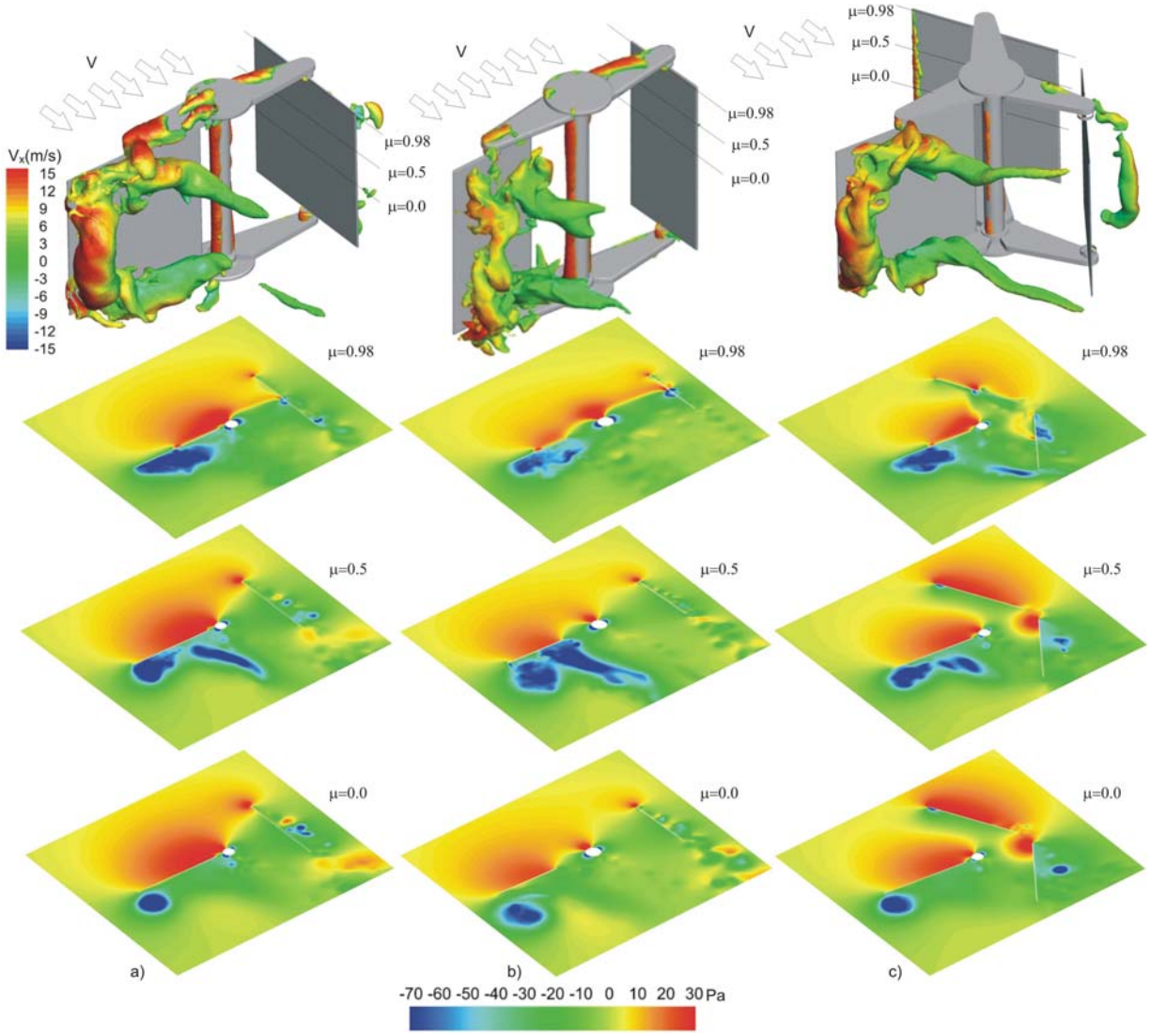

Figure 17: Instantaneous pressure Iso-surface of 70 Pa and pressure field on planes at different span-wise locations of the O-VAWT at TSR=0.4 and wind speed of 10 m/s. a) N=2, AR=1 b) N=2, AR=2 c) N=3, AR=1.

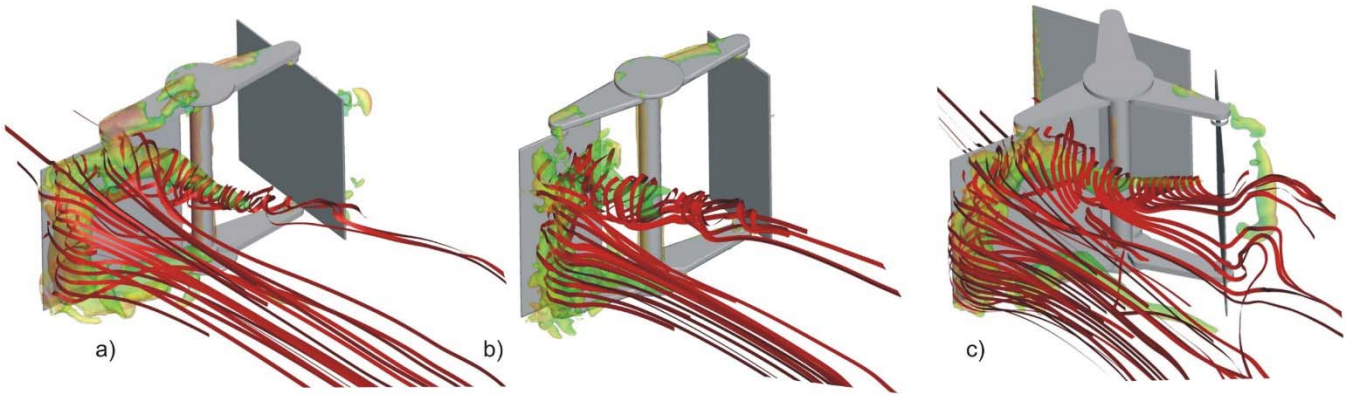

Figure 18: Streamlines around the 180°-oriented blade of the O-VAWT at TSR=0.4 and wind speed of 10 m/s. a) N=2, AR=1 b) N=2, AR=2 c) N=3, AR=1.